Geophysical Research Letters

RESEARCH LETTER
10.1029/2018GL081428

Triggering of the Mw 7.2 Hawaii Earthquake of 4 May 2018 by a Dike Intrusion

Kejie Chen[1], Jonathan D. Smith[2], Jean-Philippe Avouac[1], Zhen Liu[3], Y. Tony Song[3], and Adriano Gualandi[3]

[1]Division of Geological and Planetary Sciences, California Institute of Technology, Pasadena, CA, USA, [2]Department of Earth Sciences, University of Cambridge, Cambridge, UK, [3]Jet Propulsion Laboratory, California Institute of Technology, Pasadena, CA, USA

Key Points:
- The Mw 7.2 earthquake is a blind thrust event that most probably activated the décollement along the volcanic edifice
- Creep on the décollement and dike intrusion result in a stress unloading and guided the rupture during the Mw 7.2 earthquake
- Return period for a Mw 7.2 earthquake should be around 20 to 35 years

Supporting Information:
- Supporting Information S1
- Figure S1
- Figure S2
- Figure S3
- Figure S4
- Figure S5
- Figure S6
- Figure S7
- Figure S8

Correspondence to:
K. Chen,
whuckj@gmail.com

Citation:
Chen, K., Smith, J. D., Avouac, J.-P., Liu, Z., Song, Y. T., & Gualandi, A. (2019). Triggering of the Mw 7.2 Hawaii earthquake of 4 May 2018 by a dike intrusion. *Geophysical Research Letters*, *46*. https://doi.org/10.1029/2018GL081428

Received 22 NOV 2018
Accepted 15 FEB 2019
Accepted article online 21 FEB 2019

Abstract A Mw 7.2 earthquake struck the south flank of Kilauea, Hawaii, on 4 May 2018, following a period of volcanic unrest. To investigate its relationship with the stress changes induced by prior tectonic and magmatic activity, we model the coseismic slip distribution, preintrusion deformation, and dike intrusion using geodetic, seismic, and tsunami observations. The décollement beneath the south flank was creeping seaward by ~25 cm/year. Diking started on 20 April and led to fissure eruption on 3 May. The magmatic activity and creep resulted in an onshore U-shaped zone of stress unloading, fringed by an off-shore zone of stress buildup that apparently guided the 2018 rupture. It takes only 20 to 35 years at the preintrusion rate to accumulate a moment deficit equivalent to the moment that was released in 2018. This event falls short of balancing the moment budget since the 1975 Mw 7.7 earthquake.

Plain Language Summary As one of the most active volcanoes on Earth, Kilauea volcanos in Hawaii are responsible for various deformation sources including summit reservoirs, rift zones, décollement faults, and slumps, which result in thousands of earthquakes each year. While most of the minor earthquakes (M <4) there are related to magma movement through conduits and cracks, the causes and mechanisms for less frequent but large and devastating events, such as the 1975 Ms 7.2 Kalapana earthquake and the 1868 ~M 8 Great Kau earthquake, are still not fully understood, and only conceptual models were proposed partially due to poor observations at that time. We act to further the prior analysis to combine seismological and geodetic data sets to constrain the relationships of magmatic processes with large-scale triggered earthquakes, using the April 2018 Hawaiian eruption and the corresponding 4 May 2018 Mw 7.2 as a case study. Our results show the creep on the décollement constantly alter the stress accumulation, while dike intrusion trigger the occurrence of the large earthquakes. Besides, it will take about 20 to 35 years for such a damaging earthquake to reoccur on the décollement beneath the south flank of Kilauea.

1. Introduction

The Kilauea volcano and Eastern Rift Zone (ERZ) of Hawaii's South Island is a region of intense volcanic activity that also generates particularly large, eventually tsunamigenic earthquakes. The largest recorded earthquake there is the 1975 Mw 7.7 Kalapana earthquake (Ando, 1979; Nettles & Ekström, 2004; Owen & Bürgmann, 2006). The Kalapana earthquake mechanism was initially debated; the most widely accepted view is that it resulted from thrusting along the contact between the volcanic edifice and the underlying seafloor at a depth of 7–8 km, on a basal décollement (Thurber & Gripp, 1988; Figure 1). Thrust motion along this shallow-dipping décollement is associated with diking and rifting along the ERZ (e.g., Day et al., 2005; Ma et al., 1999). The 1975 Kalapana earthquake generated a tsunami that ran up as high as ~14 m (Goff et al., 2006). In addition, a Mw 6.2 earthquake in 1989 probably failed on the same décollement (Hooper et al., 2002). This basal décollement is also expected to produce transient aseismic slip events (Segall et al., 2006).

On 4 May 2018, a thrust earthquake of moment magnitude estimated to be Mw 6.9 occurred again on the southern flank of Kilauea (U.S. Geological Survey [USGS]/National Earthquake Information Center). It triggered a small tsunami with a maximum wave height of 40 cm (http://ptwc.weather.gov/). Both the USGS W-phase focal mechanism and the global centroid moment tensor (GCMT) suggest a dip angle of

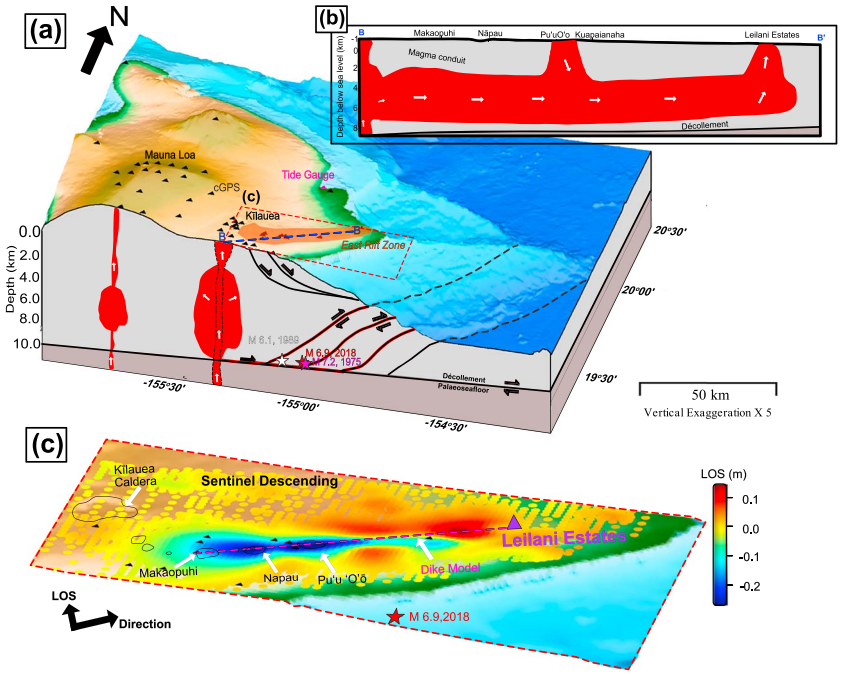

Figure 1. Simplified geological setting of the 4 May Mw 7.2 earthquake in South Island, Hawaii. (a) Three-dimensional view with internal structure modified from Morgan et al. (2003). Black triangles = continuous global position system (GPS) stations. Pink triangle = tide gauge near Hilo. (b) Cross-section approximately along the axis of the East Rift Zone showing schematically the connected magmatic system modified from Lundgren et al. (2013). (c) Interferometric Synthetic Aperture Radar (InSAR) measurements (20 April to 2 May 2018) of surface deformation along the East Rift Zone.LOS = line of sight.

20° for the north dipping plane (https://earthquake.usgs.gov/earthquakes/eventpage/us1000dyad/moment-tensor; http://www.globalcmt.org/CMTsearch.html). This dip angle, together with the shallow hypocentral depth of 5.8 km, would exclude the fact that this event activated the décollement. However, the hypocentral depth could be erroneous due to the complex velocity structure of the area (Lin et al., 2014), with difficulties in constraining the moment tensor of shallow-dipping thrust faults at shallow depth (Lay et al., 2018). Detailed analysis of the pattern of Love waves radiated by the 4 May Hawaii earthquake suggests in fact a much shallower dip angle of 2.5° to 7.5° to the NW and larger moment corresponding to Mw ~7.2 (Lay et al., 2018; Figure 1). The shallower dip angle is also suggested from the joint modeling of the available seismological and geodetic data (Liu et al., 2018).

Hereafter, we determine a source model from the joint inversion of seismic waveforms and static displacements measured from the global positioning system (GPS). We check its consistency with the tsunami waveform recorded at Hilo and examine whether this earthquake occurred on the décollement or on a splay fault (Figure 1). We then use Interferometric Synthetic Aperture Radar (InSAR) and GPS time series to place this earthquake in the context of the preceding magmatic and tectonic activity.

2. Timeline

On 17 April 2018, the Hawaiian Volcano Observatory reported elevated lava lake levels in the Pu'u'Ō'ō crater and microseismicity around the Kilauea summit (https://volcanoes.usgs.gov/volcanoes/kilauea/). The deformation and seismicity suggest that magma migrated along a dike system from beneath Kilauea to Pu'u'Ō'ō (Figure 1). On 30 April, the level of the lava lake in the Pu'u'Ō'ō crater dropped abruptly in conjunction with increased seismicity and deformation along the NE strike of the ERZ and a period of further dike propagation eastward from Pu'u'Ō'ō. By 3 May, the dike had reached the first eruption site at Leilani Estates (Figure 1). On 4 May, the Mw 7.2 earthquake struck the south flank of Kilauea at around 22:33 UTC time (Figure 1).

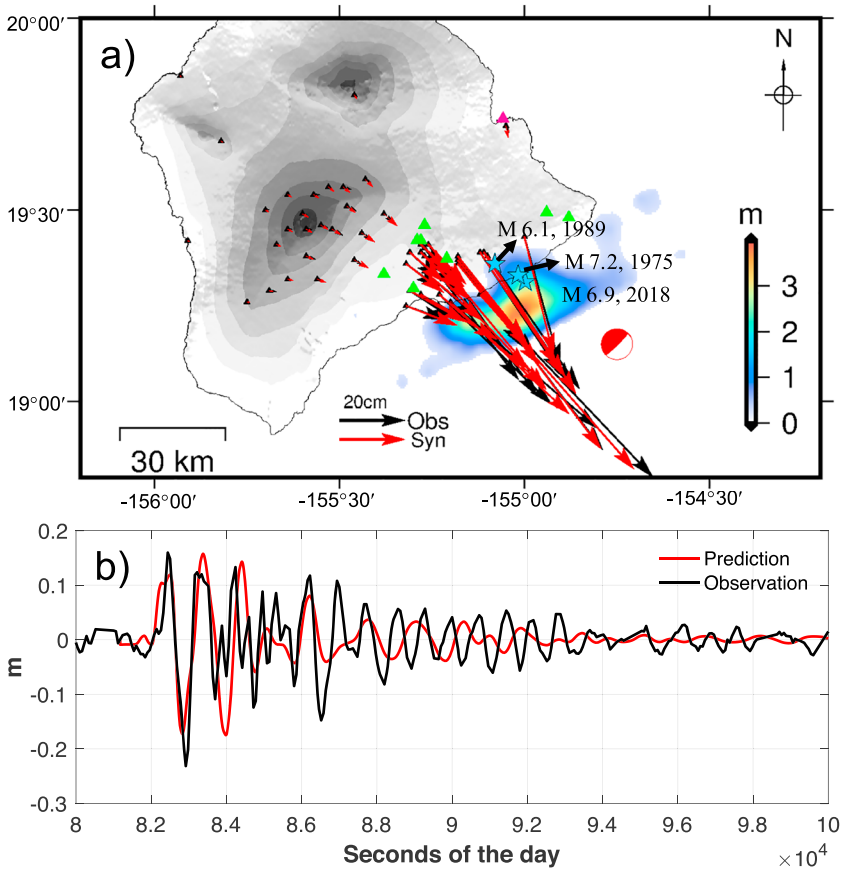

Figure 2. (a) Coseismic slip distribution of the 4 May 2018 earthquake from the joint inversion of static GPS (green triangles), strong motion (black triangles), and teleseismic waveforms. Stars = epicenters of the 1975 M 7.2, 1989 M 6.1, and 2018 Mw 7.2 earthquakes. The focal mechanism presents the faulting geometry adopted in this study, with a 245° strike and 5° NW dip. Pink triangle = tide gauge HILO2. The smooth aspect of slip model is due to the plot rendering with Generic Mapping Tools (see unfiltered version in the supporting information). (b) Observed and predicted tsunami waveforms at HILO2.

3. Coseismic Rupture

We model the 4 May 2018 earthquake from the joint inversion of 57 three-dimensional GPS static offsets, 8 three-dimensional 1-Hz strong motion velocity waveforms, and 40 1-Hz teleseismic *P* displacement waveforms. Detailed information about slip inversion can be found in Text S1 in the supporting information (Chen et al., 2016; Dziewonski & Anderson, 1981; Hartzell & Heaton, 1983; Kikuchi & Kanamori, 1982; Melgar & Bock, 2015; Zhu & Rivera, 2002). We then compare the tsunami waveform predicted by our source models with the record at the tide gauge station HILO2 (Becker et al., 2009; Leveque et al., 2011). In all inversions shown in this study the relative weighting of the different data sets is adjusted so that for each data set, residuals are of comparable amplitude relative to the noise level. In order to find an optimal solution, we vary the hypocenter depth, strike, dip angles, and rupture speed systematically (see Text S1 for details). Green's functions were calculated for a layered Earth model constrained from a local seismological study (Klein et al., 1987) (Table S1). The fault runs through the hypocenter. The hypocentral depth is varied between 5 and 9 km. The best fit to the data is obtained for a depth of 6 km, a strike of 245°, a NW dip of 5°, and a rupture speed of 1.2 km/s (Table S2). However, the variance reduction varies by up to 2% only (Table S2) if the hypocentral depth is varied between 6 and 8 km. The slip models corresponding to these solutions are very similar. Although blind, these sources produce enough seafloor displacements to fit the tsunami waveforms recorded at Hilo (Figures 2 and S1–S5). A 20° dip angle yields a much lower fit (Table S2). We therefore consider that an hypocentral depth of 8 km and a dip angle consistent with activation of the décollement offers the best compromise (Figures 2 and S1). However, this model underestimates the

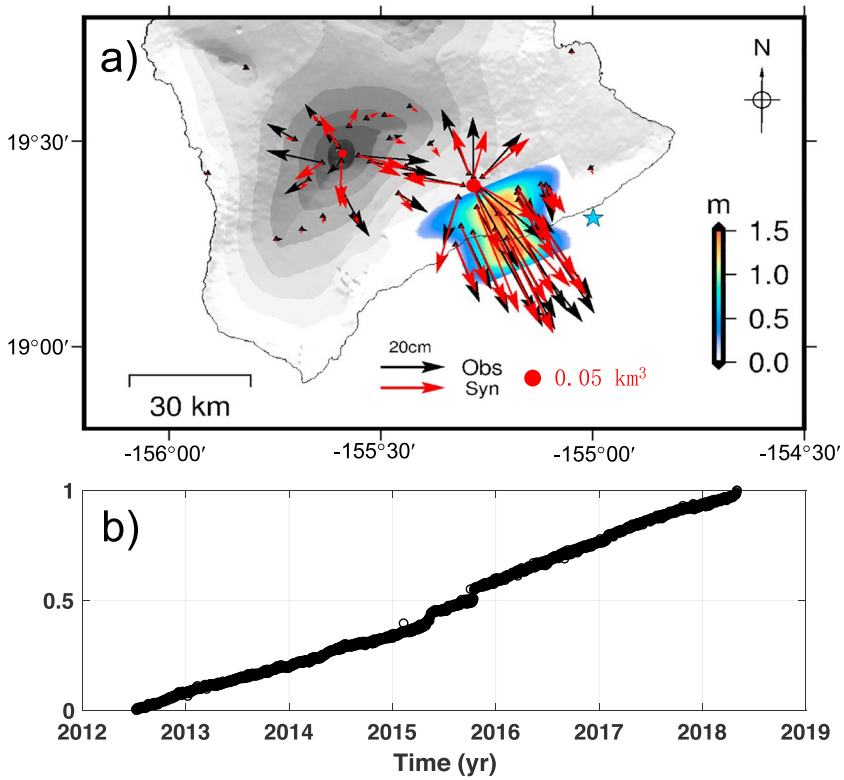

Figure 3. (a) Spatial and (b) temporal functions of the first component (black vectors) obtained from the independent component analysis of the global positioning system data from June 2012 to April 2018, which accounts for 90% of the data variance. Predicted displacements (red vectors) assuming three deformation sources: point sources of inflation below Mauna Loa and Kilauea summits (red dots) and creep on the décollement beneath the south flank of Kilauea. Blue star = epicenter of the 4 May 2018 earthquake.

horizontal components of the strong motion data but overestimates the vertical components. Further improvement of the source model would probably require a nonplanar geometry with some steeper fault segments. The moment released on steeper fault segments should be minor anyway since the nondouble component amounts to less than 3% of the global centroid moment tensor solution.

Our model suggests that the rupture front propagated bilaterally yet asymmetrically. The main asperity, with >3-m peak slip, is located ~5 km to the southwest of the epicenter. The rupture area forms an arcuate pattern that fringes the coastline offshore. According to this model, the earthquake released 7.31×10^{19} Nm, corresponding to Mw 7.17, close to the value of 8.7×10^{19} Nm estimated by Lay et al. (2018). The source time function implies that about 95% of the moment was released within 30 s. We conclude that the 4 May earthquake is a blind thrust event that most probably activated the décollement where the volcanic edifice rests over the oceanic seafloor.

4. Preintrusion Deformation

More than one century's geodetic records show that the south flank of Hawaii has been spreading seaward in association with occasional volcanic activity at Kilauea and Mauna and earthquakes (e.g., Dieterich et al., 2000; Owen et al., 1995; Swanson et al., 1976). In order to assess the possible role of magmatic and tectonic deformation in triggering the 4 May earthquake, we model the time history of deformation since the previous episode of intrusion and eruption that occurred in 2011 (Baker & Amelung, 2015). We use InSAR and GPS time series and model them using a modified version of the principal component analysis-based inversion method (Kositsky & Avouac, 2010), in which the time series are decomposed using a variational Bayesian independent component analysis (Choudrey & Roberts, 2003; Gualandi et al., 2016; Okada, 1985; see Text S2). The magmatic activity that resumed around 20 April 2018 has led to a clear change in the pattern and rate of deformation. We therefore analyze separately the periods prior and after that date.

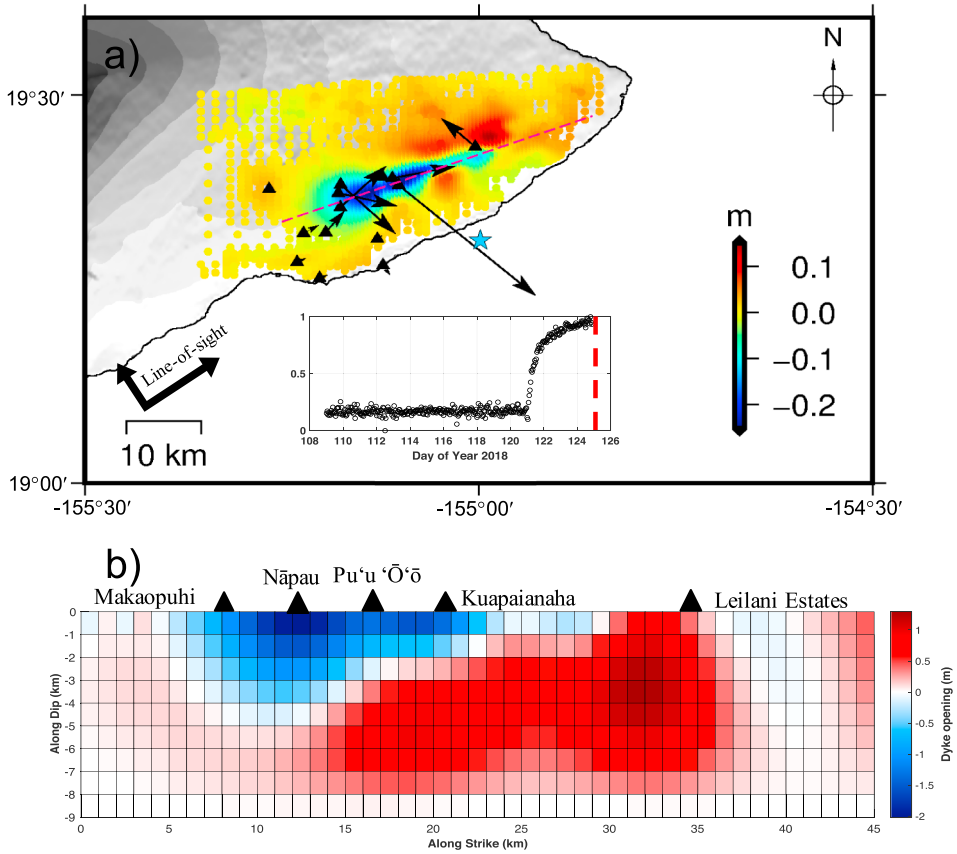

Figure 4. (a) Spatial (black vectors) and temporal (inset) functions of the first component obtained from the independent component analysis of the global positioning system (GPS) data from 20 April to 2 May 2018. Line-of-sight displacements (color shading) measured from Interferometric Synthetic Aperture Radar (InSAR) using Sentinel-1 images acquired on 20 April and 2 May. The time function depicts the temporal evolution of the dike intrusion, and the vertical red dashed line marks the Mw 7.2 earthquake on 4 May 2018. Pink line = surface projection of dike plane used in the modeling. (b) Distribution of dike opening derived from the inversion of the InSAR and GPS data. Triangles on top of it locates the approximation position of Makaopuhi, Nāpau, Pu'u'Ō'ō, and Kuapaianaha Craters and Leilani Estates.

The daily GPS displacement time series from 2012 to 20 April 2018 can be mostly explained by one component (variance reduction = 90%) with a nearly linear time evolution (Figure 3b). The spatial pattern shows outward motion from the Mauna Loa and Kilauea summits and seaward motion of the south flank of Kilauea (Figure 3). The three sources are not separated because they follow a similar linear evolution. We model this component considering point sources of magmatic expansion (Mogi, 1958) and slip on the décollement. Our solution implies creep on the décollement at ~25 cm/year on an ~30 × 30 km^2 creeping area that extends from the ERZ to beyond the coastline, and inflation of the Kilauea and Mauna Loa summits at ~4-km depth and a rate ~0.009 and ~0.005 km^3/year, respectively. The rate and extent of the creeping zone are similar to those obtained by Owen et al. (2000) based on GPS data from 1990 to 1996 or by Phillips et al. (2008), who reported rates of ~25–28 and 28 ± 7 cm/year, respectively, based on GPS data and seabottom pressure measurements from 2000 to 2004. Supply of magma into the ERZ is another source of deformation that has been considered in previous studies (Cayol et al., 2000; Owen et al., 2000; Sinnett, 2014). To check this possibility, we also model the GPS data including a dike along the ERZ (see Text S2). The rift dilates by ~7 cm/year in the best fitting model, but the fit to the GPS data is only marginally improved (variance reduction increases from 73% to 73.5%). The dike component is thus not required by the data used here.

We use InSAR and hourly GPS displacement time series from 20 April to 4 May 2018 to model the dike intrusion process. An interferogram was calculated from Sentinel-1 images acquired on 20 April and 2 May. The InSAR data provide tight spatial constraints, while the GPS data determine the temporal

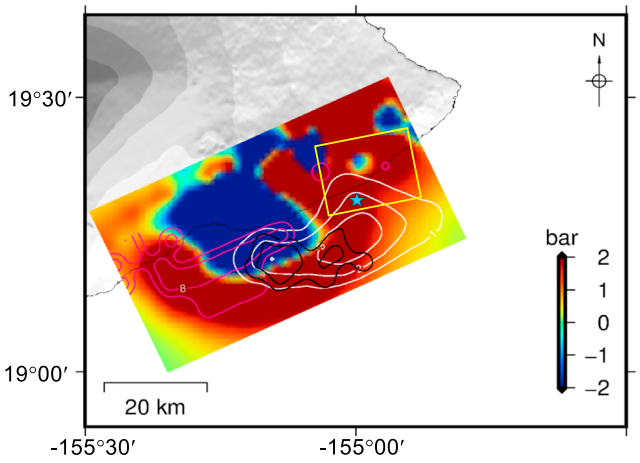

Figure 5. Seismic and aseismic slip, and Coulomb stress failure change (color shading) on the décollement between June 2012 and 4 May 2018. The color bar scale is saturated for clarity. White and pink contours outline the major rupture during the 2018 Mw 7.2 (this study) and 1975 M 7.2 earthquakes (Owen & Bürgmann, 2006). Yellow rectangle outlines the 1989 M 6.1 rupture area (Hooper et al., 2002). The black contour lines show the source area of Mw ~5.4–5.8 slow slip events (Foster et al., 2013).

resolution (see Text S3). We retain only the dominant component, as it explains 81% of the data variance. Its temporal function (Figure 4a) indicates that the deformation associated with the magmatic activity started abruptly on 1 May and slowed down gradually until the 4 May earthquake broke out (Figure 4). Our preferred model suggests that from south of Makaopuhi Crater to north of Kuapaianaha Crater, the dike closed by more than 1 m near the surface, while it opened at depth. The intrusion appeared to the surface ~9 km northeast of Kuapaianaha Crater and erupted at Leilani Estates. The rather large misfits to the GPS data are attributed to the unrealistic representation of the dike by a single vertical plane. The real system is probably nonplanar and segmented. We believe that the model is, however, sufficient to assess the stress changes in the area of the 4 May earthquake as it is distant enough not to be sensitive to the details that would be needed to fit the near-field GPS data better.

5. Discussions and Conclusions

We evaluate the stress changes on the décollement beneath the south flank of Kilauea to assess the possible influence of the magmatic and tectonic activity on the seismic rupture during this event. The stress change is quantified in terms of Coulomb failure stress change (ΔCFS), which is the quantity customarily used to assess earthquake triggering (King et al., 1994) and is defined as

$$\Delta \mathrm{CFS} = \Delta\tau_{\beta} - \mu' \Delta\sigma_{\mathrm{n}}$$

where $\Delta\tau_{\beta}$ is the shear stress change, μ' is the coefficient of effective friction, and $\Delta\sigma_{\mathrm{n}}$ is the normal stress change. We assume a uniform rake angle of 120°, consistent with the rake of the 4 May event, and the effective friction coefficient μ' is chosen to 0.35 as in Cayol et al. (2000).

Creep on the décollement and the intrusion along the ERZ caused stress changes of similar amplitudes (Figure S7). By contrast, the stress changes caused by inflation at the summit of Mauna Loa are negligible and those caused by inflation at the summit of Kilauea are even smaller (Figure S7). The epicenter lies in an area where preintrusion deformation from 2012 to April 2018 resulted in a ΔCFS increase by ~1 bar. The ΔCFS was increased further by a similar amount due to the dike intrusion (Figure 5). These values are of the same order of magnitude as the coseismic ΔCFS, which is typically interpreted to trigger aftershocks (Harris, 1998) and may have influenced the 2018 earthquake. The coseismic slip distribution during the 4 May 2018 earthquake is mostly confined to an area of increased Coulomb stress. We note, however, a small overlap with the creeping portion of the décollement where ΔCFS is negative. The overlap is probably real as the variance reduction drops from 82% to 57% if the creeping zone does not extend offshore beyond the coastline. It is interesting to note that aseismic creep on the décollement causes a U-shaped zone of negative ΔCFS around which the earthquake rupture seems to be wrapped. The rupture areas of the 1975 event (Owen & Bürgmann, 2006) and the 1989 Mw 6.2 event (Hooper et al., 2002) mostly fall in an area of positive ΔCFS (Figure 5). We therefore infer that the stress changes induced by aseismic creep along the décollement and magmatic activity along the ERZ trigger and partly control the seismic ruptures beneath the south flank of Kilauea.

Transient aseismic slip events (Foster et al., 2013; Segall et al., 2006) eventually triggered by dike intrusions, as happened in June 2007 (Brooks et al., 2008), also fall within the area of increasing Coulomb stress due to tectonic and magmatic activity and overlap with the estimated rupture area of the 4 May 2018 earthquake. The emerging picture is that slip on the décollement is mostly aseismic onshore closer to the ERZ. Higher temperature and pore pressure there could favor aseismic slip as expected if sliding is governed by rate-and-state friction (e.g., Avouac, 2015). By contrast slip on the offshore portion of the décollement is episodic with both aseismic transients and occasional large seismic ruptures. This picture is robust, no matter the choice of the décollement depth. If a shallower depth is assumed, the slip models needed to fit the

coseismic and nonseismic geodetic deformation would have the same distribution in map view with somewhat smaller amplitudes, but the same inferences can be drawn.

Our analysis allows estimating the time needed to accumulate the amount of elastic strain needed to drive damaging earthquake on the décollement beneath the south flank of Kilauea such as the 1975 and 2018 events. We assume conservation of moment over the ~65×40 km^2 fault zone that extends from the ERZ seaward to encompass the rupture areas of the 1975 and 2018 earthquakes and constant loading at the rate determined for the 2012–2018 period. This is a reasonable assumption, at least since 1990, given the similar pattern and rate of creep on the décollement found by Sinnett (2014) and Owen et al. (1995, 2000). Assuming a creep rate of 15 to 25 cm/year, the moment deficit has accumulated at 1.0 to 1.78×10^{19} Nm/year over that period. At this rate, it takes only 4 to 7 years to accumulate a moment deficit equivalent to the moment released by the 2018 Mw 7.2 earthquake. If we include the moment released by smaller earthquakes, assuming a Gutenberg-Richter frequency-magnitude distribution with a *b* value of 1, Mw 7.2 should return every 12 to 21 years. This calculation probably overestimates the contribution of smaller earthquakes to the moment budget in view of the USGS catalog, which suggests a lower *b* value, and the fact that the Bath's law is ignored (e.g., Michel et al., 2018). Given that the 2018 event is the only Mw >7 earthquake since 1975, larger-magnitude events are probably needed to balance the budget. If we assume that the budget is balanced by a Mw 7.7 event, like in 1975, it takes 20 to 35 years to accumulate the moment deficit that would be released by such an event; this estimate increases to an upper bound of 60 to 105 years if we account for the full range of smaller-magnitude events. Thus, the 2018 event did not release all strain accumulated since the 1975 Mw 7.7 earthquake, and larger events similar in size to the 1977 earthquake may be possible.

Acknowledgments
Raw GPS data for coseismic rupture inversion were downloaded from UNAVCO (available at ftp://data-out.unavco.org/pub/rinex/); GPS time series were provided by Nevada Geodetic Laboratory (available at ftp://gneiss.nbmg.unr.edu/rapids/tenv/). Strong motion and teleseimic waveforms were obtained through the Data Management Center of the Incorporated Research Institutions for Seismology. Original Sentinel-1 interferograms were provided by the European Space Agency's Sentinel-1 satellite. Tsunami records at tide gauge were collected from Global Sea Level Observing System. This research was partially funded by the National Science Foundation through grant EAR-182185. The research by Z. L. was supported by the NASA Earth Surface and Interior focus area and carried out at the Jet Propulsion Laboratory (JPL), California Institute of Technology. A. G. was supported by an appointment to the NASA Postdoctoral Program at JPL, California Institute of Technology, administered by Universities Space Research Association through a contract with NASA, in collaboration with the Agenzia Spaziale Italiana. We thank R. Burgmann for discussions and Wanpeng Feng for sharing his code on calculation of Coulomb stress change. We are grateful to Gavin Hayes (the Editor), Yong Zhang, and an anonymous reviewer for their constructive reviews. Most of the figures in this paper were prepared using Generic Mapping Tools (Wessel et al. 2013).

References

Ando, M. (1979). The Hawaii earthquake on November 29, 1975: Low dip angle faulting due to forceful injection of magma. *Journal of Geophysical Research*, *84*(B13), 7616–7626. https://doi.org/10.1029/JB084iB13p07616

Avouac, J.-P. (2015). From geodetic imaging of seismic and aseismic fault slip to dynamic modeling of the seismic cycle. *Annual Review of Earth and Planetary Sciences*, *43*(1), 233–271. https://doi.org/10.1146/annurev-earth-060614-105302

Baker, S., & Amelung, F. (2015). Pressurized magma reservoir within the east rift zone of Kīlauea volcano, Hawai'i: Evidence for relaxed stress changes from the 1975 Kalapana earthquake. *Geophysical Research Letters*, *42*, 1758–1765. https://doi.org/10.1002/2015GL063161

Becker, J. J., Sandwell, D. T., Smith, W. H. F., Braud, J., Binder, B., Depner, J., et al. (2009). Global bathymetry and elevation data at 30 arc seconds resolution: SRTM30_PLUS. *Marine Geodesy*, *32*(4), 355–371. https://doi.org/10.1080/01490410903297766

Brooks, B. A., Foster, J., Sandwel, D., Wolfe, C. J., Okubo, P., Poland, M., & Myer, D. (2008). Magmatically triggered slow slip at Kilauea volcano, Hawaii. *Science*, *321*(5893), 1177. https://doi.org/10.1126/science.1159007

Cayol, V., Dieterich, J. H., Okamura, A. T., & Miklius, A. (2000). High magma storage rates before the 1983 eruption of Kilauea, Hawaii. *Science*, *288*(5475), 2343–2346. https://doi.org/10.1126/science.288.5475.2343

Chen, K., Ge, M., Babeyko, A., Li, X., Diao, F., & Tu, R. (2016). Retrieving real-time co-seismic displacements using GPS/GLONASS: A preliminary report from the September 2015 Mw 8.3 Illapel earthquake in Chile. *Geophysical Journal International*, *206*(2), 941–953. https://doi.org/10.1093/gji/ggw190

Choudrey, R. A., & Roberts, S. J. (2003). Variational mixture of Bayesian independent component analyzers. *Neural Computation*. https://doi.org/10.1162/089976603321043766

Day, S. J., Watts, P., Grilli, S. T., & Kirby, J. T. (2005). Mechanical models of the 1975 Kalapana, Hawaii earthquake and tsunami. *Marine Geology*, *215*(1-2), 59–92. https://doi.org/10.1016/j.margeo.2004.11.008

Dieterich, J., Cayol, V., & Okubo, P. (2000). The use of earthquake rate changes as a stress meter at Kilauea volcano. *Nature*, *408*(6811), 457–460. https://doi.org/10.1038/35044054

Dziewonski, A. M., & Anderson, D. L. (1981). Preliminary reference Earth model. *Physics of the Earth and Planetary Interiors*, *25*(4), 297–356. https://doi.org/10.1016/0031-9201(81)90046-7

Foster, J. H., Lowry, A. R., & Brooks, B. A. (2013). Fault frictional parameters and material properties revealed by slow slip events at Kilauea volcano, Hawai'i. *Geophysical Research Letters*, *40*, 6059–6063. https://doi.org/10.1002/2013GL058234

Goff, J., Dudley, W. C., DeMaintenon, M. J., Cain, G., & Coney, J. P. (2006). The largest local tsunami in 20th century Hawaii. *Marine Geology*, *226*(1–2), 65–79. https://doi.org/10.1016/j.margeo.2005.09.017

Gualandi, A., Serpelloni, E., & Belardinelli, M. E. (2016). Blind source separation problem in GPS time series. *Journal of Geodesy*, *90*(4), 323–341. https://doi.org/10.1007/s00190-015-0875-4

Harris, R. A. (1998). Introduction to special section: Stress triggers, stress shadows, and implications for seismic hazard. *Journal of Geophysical Research*, *103*(B10), 24,347–24,358. https://doi.org/10.1029/98JB01576

Hartzell, S. H., & Heaton, T. H. (1983). Inversion of strong ground motion and teleseismic waveform data for the fault rupture history of the 1979 Imperial Valley, California, earthquake. *Bulletin of the Seismological Society of America*, *73*(6), 1553–1583.

Hooper, A., Segall, P., Johnson, K., & Rubinstein, J. (2002). Reconciling seismic and geodetic models of the 1989 Kilauea south flank earthquake. *Geophysical Research Letters*, *29*(22), 2066. https://doi.org/10.1029/2002GL016156

Kikuchi, M., & Kanamori, H. (1982). Inversion of complex body waves. *Bulletin of the Seismological Society of America*, *72*(2), 491–506.

King, G. C. P., Stein, R. S., & Lin, J. (1994). Static stress changes and the triggering of earthquakes. *Bulletin of the Seismological Society of America*, *84*, 935–953.

Klein, F. W., Koyanagi, R. Y., Nakata, J. S., & Tanigawa, W. R. (1987). The seismicity of Kilauea's magma system. In R. W. Decker, T. L. Wright, & P. H. Stauffer (Eds.), *Volcanism in HawaiiUnited States Geological Survey. Professional Paper 1350* (Vol. 2, pp. 1019–1185).

Kositsky, A. P., & Avouac, J.-P. (2010). Inverting geodetic time series with a principal component analysis-based inversion method. *Journal of Geophysical Research*, *115*, B03401. https://doi.org/10.1029/2009JB006535

Lay, T., Ye, L., Kanamori, H., & Satake, K. (2018). Constraining the dip of shallow, shallowly-dipping thrust events using long-period love wave radiation patterns: Applications to the 25 October 2010 Mentawai, Indonesia and 4 May 2018 Hawaii Island earthquakes. *Geophysical Research Letters*, *45*, 10,342–10,349. https://doi.org/10.1029/2018GL080042

Leveque, R. J., George, D. L., & Berger, M. J. (2011). Tsunami modelling with adaptively refined finite volume methods. *Acta Numerica*, *20*, 211–289. https://doi.org/10.1017/S0962492911000043

Lin, G., Shearer, P. M., Matoza, R. S., Okubo, P. G., & Amelung, F. (2014). Three-dimensional seismic velocity structure of Mauna Loa and Kilauea volcanoes in Hawaii from local seismic tomography. *Journal of Geophysical Research: Solid Earth*, *119*, 4377–4392. https://doi.org/10.1002/2013JB010820

Liu, C., Lay, T., & Xiong, X. (2018). Rupture in the 4 May 2018 M W 6.9 Earthquake Seaward of the Kilauea East Rift Zone Fissure Eruption in Hawaii. *Geophysical Research Letters*, *45*, 9508–9515. https://doi.org/10.1029/2018GL079349

Lundgren, P., Poland, M., Miklius, A., Orr, T., Yun, S. H., Fielding, E., et al. (2013). Evolution of dike opening during the March 2011 Kamoamoa fissure eruption, Kīlauea volcano, Hawai'i. *Journal of Geophysical Research: Solid Earth*, *118*, 897–914. https://doi.org/10.1002/jgrb.50108

Ma, K., Kanamori, H., & Satake, K. (1999). Mechanism of the 1975 Kalapana, Hawaii, earthquake inferred from tsunami data. *Journal of Geophysical Research*, *104*(B6), 13,153–13,167. https://doi.org/10.1029/1999JB900073

Melgar, D., & Bock, Y. (2015). Kinematic earthquake source inversion and tsunami runup prediction with regional geophysical data. *Journal of Geophysical Research: Solid Earth*, *120*, 3324–3349. https://doi.org/10.1002/2014JB011832

Michel, S., Avouac, J., Jolivet, R., & Wang, L. (2018). Seismic and aseismic moment budget and implication for the seismic potential of the Parkfield segment of the San Andreas Fault. *Bulletin of the Seismological Society of America*, *108*(1), 19–38. https://doi.org/10.1785/0120160290

Mogi, K. (1958). Relations between the eruptions of various volcanoes and the deformations of the ground surfaces around them. *Bulletin of the Earthquake Research Institute*, *223*(1-2), 203–212. https://doi.org/10.1016/j.epsl.2004.04.016

Morgan, J. K., Moore, G. F., & Clague, D. A. (2003). Slope failure and volcanic spreading along the submarine south flank of Kilauea volcano, Hawaii. *Journal of Geophysical Research*, *108*(B9), 2415. https://doi.org/10.1029/2003JB002411

Nettles, M., & Ekström, G. (2004). Long-period source characteristics of the 1975 Kalapana, Hawaii, earthquake. *Bulletin of the Seismological Society of America*, *94*(2), 422–429. https://doi.org/10.1785/0120030090

Okada, Y. (1985). Surface deformation due to shear and tensile faults in a half-space. *Bulletin of the Seismological Society of America*, *75*(4), 1135–1154.

Owen, S., Segall, P., Freymueller, J., Miklius, A., Denlinger, R., Árnadóttir, T., et al. (1995). Rapid deformation of the south flank of Kilauea volcano, Hawaii. *Science*, *267*(5202), 1328–1332. https://doi.org/10.1126/science.267.5202.1328

Owen, S., Segall, P., Lisowski, M., Miklius, A., Denlinger, R., & Sako, M. (2000). Rapid deformation of Kilauea volcano: Global positioning system measurements between 1990 and 1996. *Journal of Geophysical Research*, *105*(B8), 18,983–18,998. https://doi.org/10.1029/2000JB900109

Owen, S. E., & Bürgmann, R. (2006). An increment of volcano collapse: Kinematics of the 1975 Kalapana, Hawaii, earthquake. *Journal of Volcanology and Geothermal Research*, *150*(1–3), 163–185. https://doi.org/10.1016/j.jvolgeores.2005.07.012

Phillips, K. A., Chadwell, C. D., & Hildebrand, J. A. (2008). Vertical deformation measurements on the submerged south flank of Kīlauea volcano, Hawai'i reveal seafloor motion associated with volcanic collapse. *Journal of Geophysical Research*, *113*, B05106. https://doi.org/10.1029/2007JB005124

Segall, P., Desmarais, E. K., Shelly, D., Miklius, A., & Cervelli, P. (2006). Earthquakes triggered by silent slip events on Kīlauea volcano, Hawaii. *Nature*, *442*(7098), 71–74. https://doi.org/10.1038/nature04938

Sinnett, D. K. (2014). Short- and long-term deformation of Kilauea and Manua Loa volcanos, Hawai.

Swanson, D. A., Duffield, W. A., & Fiske, R. S. (1976). Displacement of the south flank of Kilauea Volcano: the result of forceful intrusion of magma into the rift zones. *U.S. Geological Survey Professional Paper*, *963*, 39 p.

Thurber, C. H., & Gripp, A. E. (1988). Flexure and seismicity beneath the south flank of Kilauea volcano and tectonic implications. *Journal of Geophysical Research*, *93*(B5), 4271–4278. https://doi.org/10.1029/JB093iB05p04271

Wessel, P., Smith, W. H. F., Scharroo, R., Luis, J., & Wobbe, F. (2013). Generic mapping tools: Improved version released. *Eos*, *94*(45), 409–410. https://doi.org/10.1002/2013EO450001

Zhu, L., & Rivera, L. A. (2002). A note on the dynamic and static displacements from a point source in multilayered media. *Geophysical Journal International*, *148*(3), 619–627. https://doi.org/10.1046/j.1365-246X.2002.01610.x